MgAl$_2$O$_4$ incorporated catalytic ceramic membrane for catalytic ozonation of organic pollutants

Haokun Bai, Lanlan Liang, Peike Cao, Haiguang Zhang, Shuo Chen, Hongtao Yu, Xie Quan [*]

Key Laboratory of Industrial Ecology and Environmental Engineering (Ministry of Education), School of Environmental Science and Technology, Dalian University of Technology, Dalian 116024, PR China

ARTICLE INFO

ABSTRACT

Heterogeneous catalytic ozonation (HCO) is a promising technology for organic pollutants removal in wastewater treatment owing to the generation of powerful but short-lived hydroxyl radicals (HO·). Herein, we incorporate MgAl$_2$O$_4$ catalysts on the surface of ceramic membrane pores (MgAl membrane) to enhance HO· utilization and promote pollutant degradation under spatial confinement. The MgAl catalytic membrane achieved a removal efficiency of 74.0% for ibuprofen (5 mg/L) with 68.8% total organic carbon (TOC) removal, and the pollutant removal efficiency maintained over 67% in 25 h. Electron paramagnetic resonance (EPR) and scavenging experiments revealed that HO· played the dominant role in pollutant degradation. The catalyst surface hydroxyl groups were identified as active sites to effectively generate HO· via ozone decomposition. This work provides a viable strategy to achieve efficient pollutant degradation in wastewater treatment under spatial confinement in a membrane configuration.

1. Introduction

Advanced oxidation processes (AOPs) have been widely employed in industrial and municipal wastewater treatment. Examples of typical AOPs include photocatalysis [1], Fenton technology [2], persulfate [3,4] and ozone oxidation [5,6]. Among these technologies, heterogeneous catalytic ozonation (HCO) is considered as a powerful technique for efficient destruction of recalcitrant contaminants [7,8]. In the HCO process, ozone molecules are initially adsorbed on the active site of the catalyst and transferred into highly oxidizing hydroxyl radicals (HO·), which would diffuse into the bulk phase and degrade organic pollutants via nonselective oxidation. Many studies have focused on developing new catalysts with excellent HO· production efficiency to enhance HCO [6,9,10]. However, with a short lifetime of ~10 μs, HO· can only travel ~100 nm from the catalyst's surface [11], which limits its mass transfer into the bulk phase, significantly lowering HO· availability and degradation efficiency. Chen's study showed that the concentration of HO· was found to be negligibly low beyond 200 nm from the catalyst's surface [12]. In recent years, researchers observed that when HO· was restricted within its critical diffusion distance in a confined nanospace, the availability of HO· can be significantly improved. For example, by confining HCO in anodized aluminum oxide nanochannels, the HO·

exposure was greatly enhanced with an R$_{ct}$ (ratio of HO· and O$_3$ exposure) value of up to 8.0×10^{-5} in 10 nm nanochannels, which was 2–3 orders of magnitude higher than batch systems [11]. Therefore, it is an effective strategy to boost HO· utilization efficiency and achieve rapid pollutant degradation by conducting HCO through spatial confinement.

Ceramic membranes are widely applied in wastewater treatment owing to their high chemical resistance and strong mechanical properties [13–15]. The nanopores of ceramic membrane provide suitable space for effectively encapsulating HO·, thereby enhancing its availability and promoting efficient degradation of pollutants. Incorporating catalysts with ceramic membranes can significantly increase the production and utilization efficiency of HO·, leading to enhanced HCO kinetics. Yang et al. prepared a Mn$_2$O$_3$ catalytic ceramic nanofiber membrane (referred to as Mn@CNMs). The Mn@CNM coupled with ozonation could achieve a removal efficiency of 81.3% for sulfamethoxazole (SMX) during a 7-h continuous operation [16]. He et al. fabricated a novel catalytic ceramic membrane impregnated with MnMe oxide (Me=Fe, Co, Fe). Among them, MnCe ceramic membrane exhibited the highest atrazine degradation efficiency (99.99%) under 4 mg/L ozone concentration. Moreover, it maintained a degradation efficiency of over 85% throughout 5 reuse cycles [17]. A Ce/TiO$_x$-functionalized catalytic ceramic membrane was developed by Lee et al. by

impregnation and dip-coating method. The catalytic membrane could achieve N, N-diethyl-m-toluamide (DEET) degradation up to 40%, while simultaneously achieving 35% TOC removal within 3 cycles [18]. As a type of spinel oxides (AB$_2$O$_4$), MgAl$_2$O$_4$ are earth abundant, chemically stable, and most importantly, possess surface hydroxyl groups (Me-OH) which are critical for ozone decomposition to produce HO·[6]. Therefore, we anticipated that the incorporation of MgAl$_2$O$_4$ within membrane pores and its combination with HCO could enable efficient radical utilization and pollutant degradation in wastewater treatment.

In this work, we successfully fabricated a MgAl$_2$O$_4$ catalytic ceramic membrane (denoted as MgAl membrane). The MgAl$_2$O$_4$ nanoparticles were introduced evenly on the surface and within the pores of ceramic membrane. The MgAl catalytic membrane couple with ozonation (CMCO) exhibited much higher removal efficiency (74.0%) for the refractory pollutant ibuprofen (IBU) compared to sole ozonation (42.7%) and Al$_2$O$_3$ membrane (52.1%). HO· was identified as the dominant reactive oxygen species for pollutants removal in MgAl CMCO. In-situ FTIR results revealed that surface hydroxyl groups on the catalysts served as the active sites to generate HO· via O$_3$ decomposition.

2. Materials and methods

2.1. Chemicals and materials

Al$_2$O$_3$ powder (corundum, 400 nm), humic acid (HA), ibuprofen (C$_{13}$H$_{18}$O$_2$, IBU) and indigo carmine (C$_{16}$H$_8$N$_2$Na$_2$O$_8$S$_2$) were purchased from Shanghai Aladdin company. Citric acid (C$_6$H$_8$O$_7$) was obtained from Tianjin Tianda Chemical Reagent Company. Polyvinyl alcohol (PVA) was supplied by Sinopharm Chemical Reagent Co. Ltd. Glycerol (C$_3$H$_8$O$_3$) were purchased from Tianjin Damao Chemical Reagent Company. Pluronic F127,5,5-Dimethyl-1-pyrroline (DMPO), 2,2,6,6-tetramethyl-4-piperidone (TEMP) was obtained from Sigma-Aldrich. All the chemicals were used without further purification. The O$_3$ gas was generated by O$_3$ generator (COM-AD-01, Anshan Anseros Environmental Protection Co. Ltd, Anshan, China) supported by pure oxygen.

2.2. Preparation of MgAl ceramic membranes

The MgO powder was synthesized by citric acid-assisted sol-gel method. Briefly, equal mole amount (30 mmol) of Mg(CH$_3$COO)$_2$·4 H$_2$O and citric acid were dissolved into 100 mL ultrapure water under magnetic stirring to form precursor solution. The solution was heated at 90 ℃ until uniform and transparent gel was formed. Then the sample was dried at 100 ℃ for 6 h and calcined at 550 ℃ for 2 h with a heating rate of 2 ℃/min. After cooling to room temperature, the sample was collected, washed and grinded for further experiment.

The MgAl ceramic membrane was prepared by a ball-milling, pressing and calcination process. First, a certain amount of Al$_2$O$_3$ powder, PVA (0.9%) solution and MgO (5 wt%, 10 wt%, 15 wt%, 20 wt% of Al$_2$O$_3$) were added into the corundum ball-milling bowl. The membrane samples with different catalyst loading were denoted as MgAl-5, MgAl-10, MgAl-15, MgAl-20, respectively. Then the mixture was ball-milled by a planetary ball-milling machine (QM-3SP4, Nanjing NanDa Instrument Plant) assisted by ZrO$_2$ grinding balls. After overnight drying, the mixed powder was pressed under the hydraulic pressure of 10 MPa for 60 s in a disc membrane mold to obtain the green-pressing membrane. Finally, the as-prepared membranes were put into muffle furnace and calcined at 1000 ℃ for 2 h with a heating rate of 5 ℃/min. In addition, the Al$_2$O$_3$ membrane was prepared according to the same process above without the addition of MgO.

2.3. Characterization

The surface morphology and crystal lattice information of catalytic ceramic membrane were investigated by S-4800 Field Emission Scanning Electron Microscope (SEM, Hitachi, Japan) with energy dispersive

spectrum (EDS) and High-Resolution Transmission Electron Microscopy (HR-TEM) (TEM, Thermo scientific, USA). The crystal structure of ceramic membranes was analyzed by X-Ray Diffractometer (XRD, Rigaku, Japan) equipped with monochromatic Cu-Kα radiation source. The Brunauer Emmett-Teller (BET) specific surface area was determined by BET analyzer (Quadrasor-SI, USA). Electron paramagnetic resonance (EPR) spectra was obtained on Bruker (A200–9.5/12, Germany) to verify the existent type of radicals in catalytic ozonation system. X-ray photoelectron spectroscopy (XPS, k-Alpha+, Thermo Fisher Scientific Inc, USA) was used to determine the chemical states of elements in ceramic membranes. The surface charge of catalysts in water with different pH was measured on a zeta potential analyzer (ZS90, Malvern, UK). The ATR-FTIR analysis was conducted by Thermo Scientific Nicolet iS20 with DTGS detector. Fluorescence spectrophotometer (F-4500; Hitachi) was used to record the fluorescence spectra of 2-hydroxyterephthalic acid.

2.4. Experimental setup

The HCO performance of different ceramic membranes coupled with ozonation (CMCO) was evaluated in a membrane module in a cross-flow configuration (Fig. S1). The O$_3$ stock solution was prepared by bubbling O$_3$ gas (0.2 L/min) in 4 ℃ ultrapure water which was controlled by thermostat water bath prior to experiment. After ozone saturation, the O$_3$ stock solution and the feed water solution were pumped by two peristaltic pumps at 1:1 volumetric ratio and mixed together before introduced into the membrane module. The flow rate of the peristaltic pumps was set at 1.0 mL/min. The membrane filtration velocity was set at 0.1 mL/min by controlling the cross-flow valve. During HA membrane fouling tests, the permeate was collected and weighed by an electronic weight balance at specific time intervals. The water flux of the membrane (*J*) was calculated as follows:

$$J = \frac{\Delta V}{A \times \Delta t \times \Delta P}$$

Where *J* is the water flux (L m^{-2} h^{-1} bar^{-1}), ΔV (m^3) is the volume of the permeate, *A* (m^2) is the effective membrane filtration area, Δt is the filtration time, ΔP is the transmembrane pressure.

The retention time (t) was calculated as follows:

$$t = \frac{Q}{V} = \frac{J \times A \times \Delta P}{S \times h \times \rho}$$

Where Q (L h^{-1}) is the flow rate, V (m^3) is the inner volume of the ceramic membrane, S (m^2) is the filtration area of the ceramic membrane, h (m) is the thickness of the ceramic membrane, ρ (%) is the porosity of the membrane. Thus, the retention time within ceramic membranes was calculated as 180 s.

2.5. Analytical method

Ibuprofen was selected as a test pollutant and its concentration was determined by high performance liquid chromatography (HPLC, Waters) equipped with a UV detector (Photodiode Array Detector 2996) at the wavelength of 223 nm with a C18 column. The mobile phase was acetonitrile and 0.1% formic acid water solution (V: V=70:30) at the flow rate of 0.8 mL/min. The total organic carbon (TOC) was detected by TOC analyzer (Analytikjena, multi-N·C®2100, Germany). The liquid O$_3$ concentration was determined by the indigo method [19]. The leaching concentration of metal ions in permeate was analyzed by Inductively Coupled Plasma (ICP, AVIO 500, PerkinElmer, USA) Spectroscopy. The analytical methods for other pollutants by HPLC were presented in Table S1.

3. Result and discussion

3.1. Characterization of MgAl membranes

The XRD patterns of different membranes were shown in Fig. 1a. The standard peaks (19.0°, 31.3°, 36.9°, 38.6°, 44.9°, 65.3°, 74.1°) are indexed to PDF card#21-1152, which corresponds to the (111), (220), (311), (222), (400), (440), (620) lattice plane of $MgAl_2O_4$. The other peaks corresponded to the representative peaks of aluminum oxide (PDF card#78-2426). As the loading amount increased, the representative peaks of $MgAl_2O_4$ became sharp and more intense, which suggested higher crystallization degree of the catalyst. The peaks located at 30.1° and 50.2° were attributed to the ZrO_2 introduced during the ball-milling procedure. The XPS survey spectra of Al_2O_3 and 15-MgAl membranes were presented in Fig. S2, which verified the existence of Al, O and Mg elements in the membrane. Fig. 1b-d showed the Al 2p, O 1 s and Mg 1 s spectra, respectively. The Al 2p spectrum of $MgAl_2O_4$ membrane was deconvolved into two peaks at 73.8 eV and 74.5 eV, which corresponded to the normal and inversed spinel structure in reported literature [20,21]. The O 1 s peak was deconvoluted into two peaks located at 531.1 eV and 530.4 eV, which could be attributed to lattice oxygen O^{2-} (O_{latt}) and surface-adsorbed oxygen (O_{ads}) species, respectively [22]. The XRD and XPS results verified the in-situ generated spinel phase of $MgAl_2O_4$.

The photograph of different catalytic ceramic membranes was presented in Fig. S3. The SEM images of different ceramic membranes were presented in Fig. 2. As can be seen from Fig. 2a-e, the pores of ceramic membranes were formed by the accumulation of nanoparticles. The morphologies of MgAl ceramic membranes were not influenced by loading $MgAl_2O_4$ owing to the uniform distribution of $MgAl_2O_4$ across the surface and nanopores inside MgAl membranes. The cross-sectional EDS mappings of Al_2O_3 and MgAl membrane were performed to visualize the element distribution of different membranes. Fig. 3a-d showed that only O and Al existed in Al_2O_3 membrane. After catalyst

incorporation (Fig. 3e-h), the EDS images revealed a structure with uniform distribution of Mg elements on the cross-section of 15-MgAl membrane, which indicated that $MgAl_2O_4$ nanoparticles were successfully incorporated into the nanopores of ceramic membrane.

Fig. S4 showed the TEM images of $MgAl_2O_4$ nanoparticles with the size of about 20 nm. The standard lattice space of 0.466 nm, 0.285 nm, 0.142 nm were observed, corresponding to the (111), (220) and (440) crystal plane of $MgAl_2O_4$, respectively. The atomic force microscopy (AFM) was employed to assess the surface roughness of different ceramic membranes. The three-dimensional AFM images in Fig. S5 showed similar topography of different membranes, while 15-MgAl membrane was smoother than original one. It was reported that a smooth membrane surface could be beneficial for its antifouling performance [23]. The average roughness Ra of 15-MgAl membrane was 30.8 nm, significantly lower than that of Al_2O_3 membrane (R_a=120.7 nm). The lower Ra value was probably attributed to the in-situ generated $MgAl_2O_4$ nanoparticles which occupied the surface defects of accumulated Al_2O_3 particles [24]. The N_2 adsorption-desorption isotherm presented in Fig. S6 exhibited type IV isotherms for all samples. With an increase in catalyst loading amount, the BET specific surface area increased from 14.7 m^2/g (Al_2O_3 membrane) to 22.5 m^2/g (20-MgAl membrane) (Table S2), which provided more active sites for adsorption and decomposition of ozone molecules. The contact angles of the membranes were measured to evaluate their hydrophilic properties. The data in Fig. S7 showed that all ceramic membranes had a contact angle of near 20°, suggesting that they all possessed a hydrophilic surface, which could facilitate water transport and prevent hydrophobic contaminants from attaching [25]. The water flux of different ceramic membranes was listed in Fig. S8.

3.2. Catalytic performance of MgAl CMCO

The HCO performance of MgAl membranes along with Al_2O_3 membrane was evaluated taking ibuprofen as a target pollutant. The
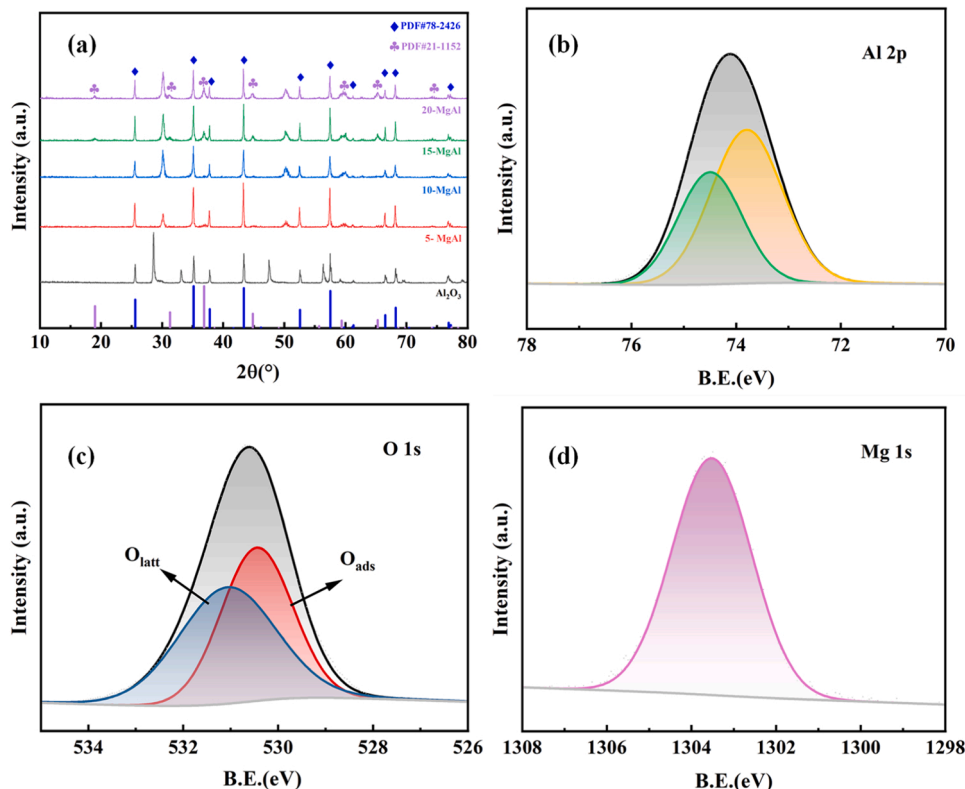

Fig. 1. (a) XRD diffraction patterns of different ceramic membranes; (b) Al 2p spectrum, (c) O 1 s spectrum and (d) Mg 1 s spectrum of 15-MgAl membrane.
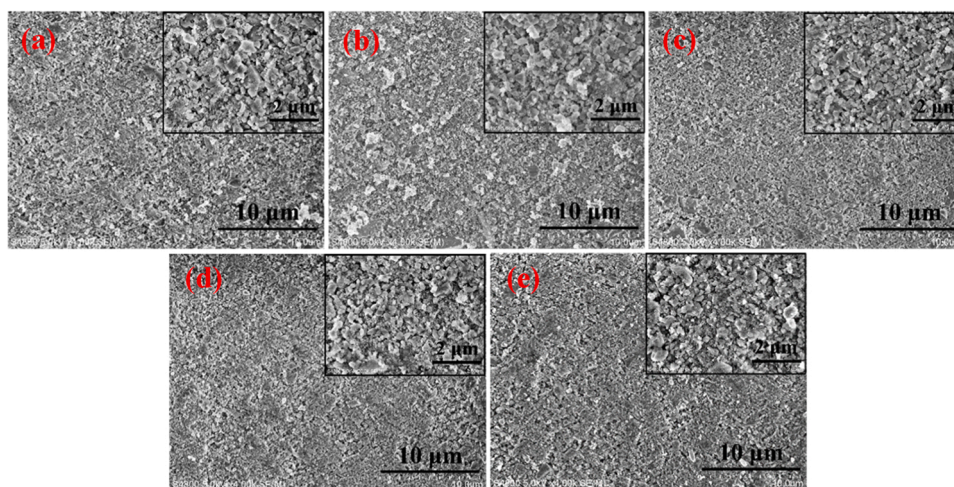
Fig. 2. SEM images of the surface of (a) Al$_2$O$_3$ membrane, (b) 5-MgAl membrane, (c) 10-MgAl membrane, (d) 15-MgAl membrane, (e) 20-MgAl membrane.
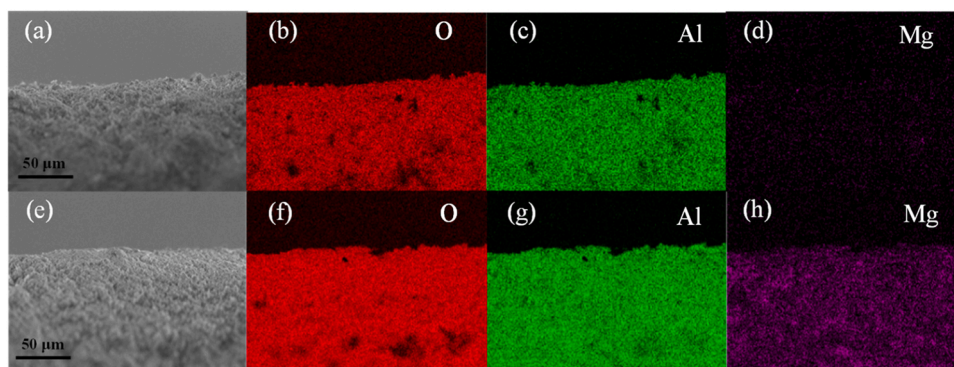

Fig. 3. EDS mappings and spectrum of the cross-section image of (a-d) Al$_2$O$_3$ membrane and (e-h) 15-MgAl membrane.

experiments were all conducted in a continuous cross-flow mode with a constant feed water flow through the membrane module. We first carried out control experiments without ozone to investigate the contribution of pollutant removal by membrane adsorption. As shown in Fig. S9, the pollutant adsorption by different catalytic membranes were not significant (<10%). Fig. 4a showed the HCO performances of MgAl CMCO. The ibuprofen removal was relatively low by ozone alone (42.7 and Al$_2$O$_3$ CMCO (52.0%). For MgAl CMCO, the removal of ibuprofen increased significantly with catalyst loading and followed the order of 5-MgAl (62.6%) < 10-MgAl (68.3%) < 20-MgAl (69.5%) < 15-MgAl (74.0%) CMCO. Besides, 15-MgAl CMCO also exhibited 68.8 % TOC removal (Fig. S10) which was significantly higher than sole ozonation (6.2%). The excellent degradation and mineralization ability of MgAl CMCO could be attributed to both high HCO performance of MgAl$_2$O$_4$ and spatially-confined membrane pores for effective utilization of HO· to achieve efficient pollutant degradation. In view of catalytic performance, the 15-MgAl membrane was chosen for further experiments.

The effect of ozone concentration on ibuprofen removal was investigated by changing the concentration of ozone in stock solution. As illustrated in Fig. 4b, the degradation efficiency of ibuprofen was enhanced with an increase in ozone concentration. As the ozone concentration increased from 1.5 mg/L to 3 mg/L, the ibuprofen removal was enhanced from 59.9% to 90.0% and then slightly increased to 92.8% as ozone concentration continued to increase to 4 mg/L. The inlet and outlet ozone concentration were monitored to investigate the ozone decomposition efficiency in Al$_2$O$_3$ and 15-MgAl CMCO. As shown in Fig. S11, the ozone utilization efficiency for 15-MgAl membrane was higher (95.0%) than that of Al$_2$O$_3$ membrane (78.8%). The enhanced

ozone decomposition could be attributed to more active sites in the pores of 15-MgAl membrane by the incorporation of MgAl$_2$O$_4$ catalyst. In addition, the specific O$_3$ consumption by 15-MgAl membrane was calculated to be 0.776 g O$_3$ g^{-1} TOC removed. Table 1 summarized the specific O$_3$ consumption of previous works based on CMCO processes. The specific O$_3$ consumption was ranging from 1.13 to 8.0 g O$_3$ g^{-1} TOC under similar experimental conditions. In comparison with previous results, the energy-efficient MgAl CMCO process offers a promising perspective for practical wastewater treatment.

The impact of solution pH on the degradation of ibuprofen was investigated, with the results displayed in Fig. 4c. It showed that the removal efficiency showed an increase from 67.5% to 77.9% as the pH value decreased from 9.0 to 3.0, which suggested that the MgAl membrane could achieve effective degradation efficiency over a broad pH range. The catalytic performance of CMCO system depended on the surface properties of catalysts, i.e. the surface hydroxyl groups, whose charge was influenced by solution pH:

$$MeOH_2^+ \leftrightarrow MeOH + H^+, K_{a1}^{int} \tag{1}$$

$$MeOH \leftrightarrow MeO^- + H^+, K_{a2}^{int} \tag{2}$$
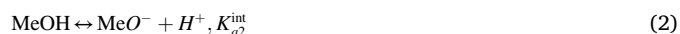
where K_{a1}^{int} and K_{a2}^{int} are the intrinsic ionization constants.

According to the zeta potential test, 15-MgAl membrane exhibited a pH$_{pzc}$ value of 9.2 (Fig. S12), which was higher than that of Al$_2$O$_3$ membrane (7.0). The fraction of different surface hydroxyl species on both membranes were also calculated. As shown in Fig. S13, the protonated surface hydroxyl groups Me-OH$_2^+$ in 15-MgAl membrane played a dominant role in acidic environment. However, their predominance
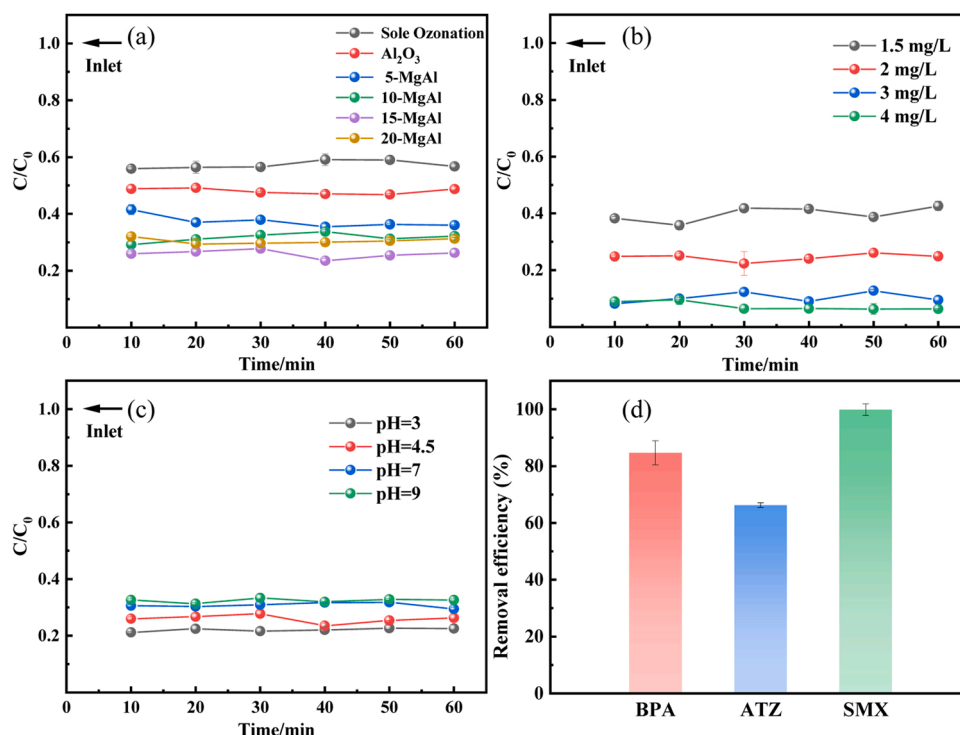
Fig. 4. (a) Catalytic performance by different CMCO on ibuprofen removal. Conditions: $C_{Ibuprofen}$= 5 mg/L; ozone dosage= 2 mg/L; Water flux= 19.1 LMH; Effect of (b) ozone concentration and (c) pH on ibuprofen removal; (d) Degradation of different pollutants by 15-MgAl CMCO. Conditions: $C_{pollutants}$= 5 mg/L; ozone dosage= 2 mg/L; Water flux= 19.1 LMH.

Table 1
Specific ozone consumption and comparison among other CMCO processes.

HCO system	Inlet TOC and O_3	Specific O_3 consumption (g O_3 g^{-1} TOC)	Reference Work
Ce-ceramic membrane	TOC= 6 mg/L (CA+BPA+BTZ)	2.1	[26]
Mn-ceramic membrane	O_3 = 5 mg/L	8.0	
Ce/TiOx ceramic membrane	TOC= 4 mg/L (DEET) O_3 = 5 mg/L	1.4	[18]
cementitious membrane	TOC= 0.92–6.9 mg/L (p-CNB) O_3 = 2.5 mg/L	1.13–3.46	[27]
Mn oxide ceramic membrane	TOC= 0.046 mg/L (p-CNB) O_3 = 0.5 mg/L	8.69	[28]
MnO_2-CNTs membrane	TOC= 4.29–7.15 mg/L (MB) O_3 = 5 mg/L	1.2	[29]
MgAl ceramic membrane	TOC= 4.2 mg/L (Ibuprofen) O_3 = 2 mg/L	0.776	This work

declined as pH reached 9, aligning with the influence of pH on the catalytic activity of 15-MgAl CMCO. The protonated surface hydroxyl groups could act as Lewis acid sites that were beneficial for the adsorption and activation of ozone molecules [30]. Consequently, as the pH decreased, the Me-OH$_2^+$ became more dominant which was beneficial for promoting ozone decomposition to generate HO· for non-selective oxidation of pollutants [31].

3.3. Stability and universality of MgAl CMCO system

A long-term catalytic experiment was conducted to evaluate the stability of 15-MgAl membrane. As shown in Fig. S14, the removal

efficiency of ibuprofen for 15-MgAl membrane maintained above 67% in 25 h. The leached Al^{3+} and Mg^{2+} ions (0.14 mg/L and 0.6 mg/L, respectively) took only 0.001% and 0.028% mass fraction of 15-MgAl membrane, which proved its excellent stability. Fig. 4d shows the removal efficiency of different representative organic pollutants, including bisphenol A (phenols), atrazine (pesticides) and sulfamethoxazole (antibiotics). The 15-MgAl CMCO system achieved high removal efficiency of 84.7%, 66.3% and 99.9% for bisphenol A, atrazine and sulfamethoxazole, respectively. It could be inferred that the MgAl CMCO system was effective in degrading pollutants with different structures.

3.4. Anti-fouling performance of MgAl CMCO

To evaluate the anti-fouling performance of both Al_2O_3 membrane and 15-MgAl membrane, humic acid (HA) was selected as a representative foulant for membrane fouling tests. As shown in Fig. S15, the HA rejection rate of 15-MgAl membrane (98%) and Al_2O_3 membrane (91%) was higher than that of ozonation alone (49%), suggesting that HA molecules could be effectively intercepted by membrane filtration. However, this caused a gradual increase in transmembrane pressure which led to the decrease of membrane flux (Fig. 5a) because HA can accumulate on the surface of ceramic membranes to cause severe membrane fouling [32,33]. However, when HA filtration was conducted in 15-MgAl CMCO system, the membrane fouling was significantly alleviated, and the flux recovery of 15-MgAl membrane was more pronounced than that of Al_2O_3 membrane. Besides, actual petrochemical wastewater (COD=92.7 mg/L, TOC=27.8 mg/L) was also tested for membrane fouling. As illustrated in Fig. 5b, similarly, a higher flux recovery rate was observed for 15-MgAl CMCO compared to Al_2O_3 CMCO. These results suggested that 15-MgAl CMCO system showed excellent HA rejection and anti-fouling properties duo to the high radical generation within the pores of 15-MgAl membrane.
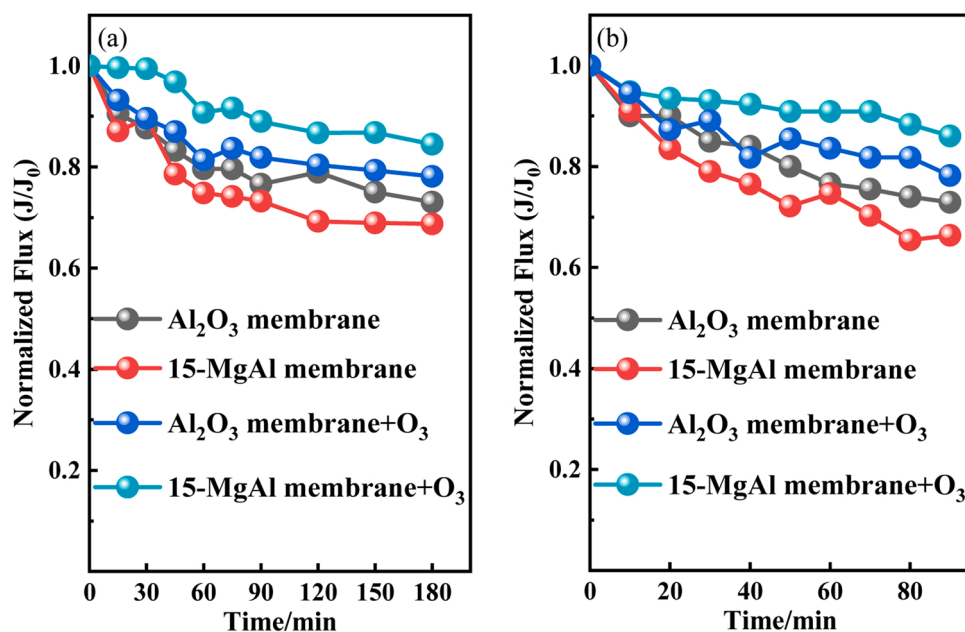
Fig. 5. The changes of normalized fluxes of Al_2O_3 membrane and 15-MgAl membrane coupled with and without ozone during the filtration of (a) HA solution and (b) petrochemical wastewater. Conditions: $C_{HA}= 5$ mg/L; ozone dosage= 2 mg/L.

3.5. Mechanism discussion

3.5.1. Identification of ROS in CMCO system

To identify the existing ROS in MgAl CMCO, EPR tests were carried out taking both DMPO and TEMP as trapping agents. The 5,5-Dimethyl-1-pyrroline (DMPO) was used for the detection of HO· and O_2^- with water and methanol as the solvent, respectively. As seen in Fig. 6a, the characteristic peak of DMPO-HO· with the height intensity ratio of 1:2:2:1

($α_N =14.87$ G $α_H=14.87$ G) was shown in 15-MgAl CMCO, verifying the existence of HO·. However, the EPR signals of DMPO-O_2^- were not observed in the system. In addition, the TEMP-$^1O_2$ peak intensity was attenuated compared with background signal (Fig. S16), which implied that $^1O_2$ may not participated in 15-MgAl CMCO. To further validate the generation of HO·, fluorescence spectroscopy was employed to detect HO· in different systems using terephthalic acid (TA) as the probe molecule under an excitation wavelength of 315 nm. TA reacts with HO·
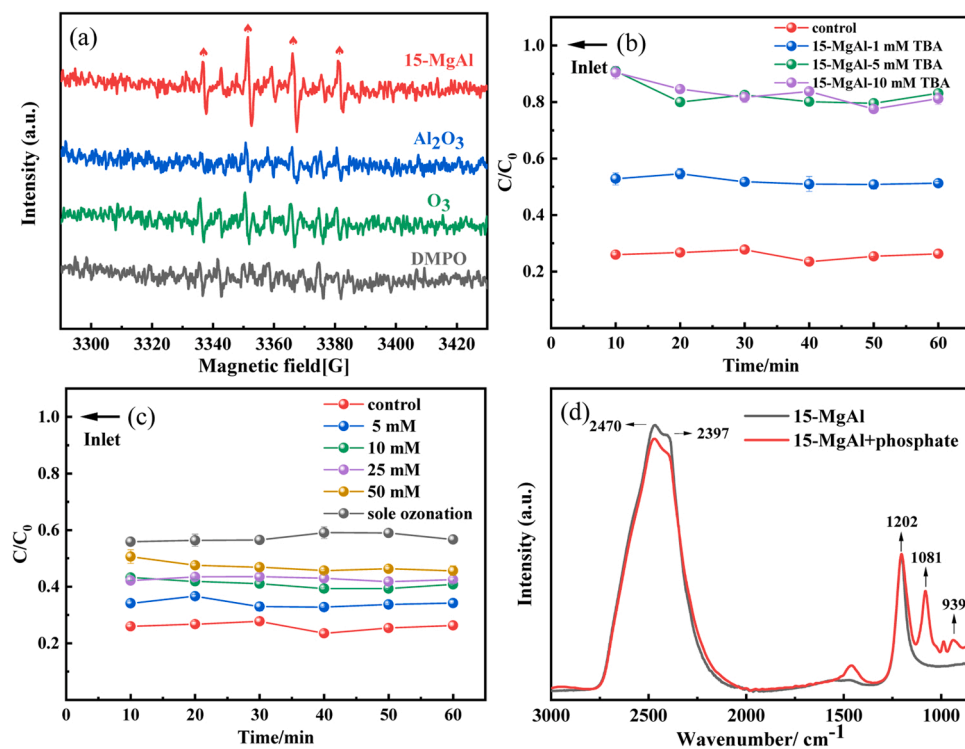

Fig. 6. (a) EPR spectra of HO· using DMPO as the trapping agent. (b) Effect of TBA on ibuprofen removal by 15-MgAl CMCO; (c) Effect of phosphate on ibuprofen removal by 15-MgAl CMCO. Conditions: $C_{Ibuprofen}= 5$ mg/L; ozone dosage= 2 mg/L; Water flux= 19.1 LMH. (d) ATR-FTIR spectra of 15-MgAl/D_2O with/without phosphate.

to produce fluorescent 2-hydroxyterephthalic acid (2-HTA), whose fluorescent peak intensity is proportional to HO· concentration [34]. In Fig. S17, the peak appeared at approximately 426 nm, and the fluorescence signal of 15-MgAl CMCO was higher than that of Al_2O_3 CMCO and sole ozonation. The fluorescence spectroscopy measurements were consistent with the EPR results above. It could be concluded that the MgAl CMCO could generate more HO· to boost the degradation of pollutants in water.

We further employed tertiary butanol (TBA) as HO· scavenger to explore the contribution of ozone and HO· since TBA could effectively scavenge HO· ($k = 6 \times 10^8$ M^{-1} s^{-1}) in the solution while hardly reacts with ozone molecules ($k = 3 \times 10^{-3}$ M^{-1} s^{-1} [35]). For sole ozonation, the addition of TBA didn't contribute to the removal of ibuprofen (Fig. S18), suggesting that the organic molecules were removed by sole ozonation and almost no HO· was involved. For 15-MgAl membrane, as the amount of TBA increased from 0 to 10 mM, the removal efficiency significantly declined from 74.0% to 18.2% (Fig. 6b). These results further confirmed that the HO· generated inside the nanopores of catalytic membrane played a dominant role in MgAl CMCO system.

3.5.2. Probing surface hydroxyl groups with phosphate and ATR-FTIR

Phosphate serves as a strong Lewis base which exhibits high affinity towards the surface hydroxyl groups on the catalyst, and hinder the interaction of ozone with the Lewis acid sites on catalyst's surface [6, 36]. As shown in Fig. 6c, the addition of phosphate distinctly inhibited the degradation of ibuprofen. As the amount of phosphate increased from 5 mM to 50 mM, the removal of ibuprofen decreased from 74.0% to 54.5%. The ATR-FTIR was further conducted to investigate the interaction between surface hydroxyl groups and phosphate. Instead of H_2O, D_2O was employed to distinguish it from the surface hydroxyl groups of 15-MgAl membrane. As illustrated in Fig. 6d, the adsorption peak intensity of MeO-D at 2470 cm^{-1} and hydrogen bonded D_2O at 2397 cm^{-1} were attenuated in the presence of phosphate while two new peaks appeared at 1081 cm^{-1} and 939 cm^{-1}, which were attributed to phosphate vibration [6,37]. It could be inferred that phosphate substituted the surface hydroxyl groups of 15-MgAl membrane and inhibited its interaction with ozone molecules. These results above indicated that the surface hydroxyl groups on the catalyst acted as the active sites in MgAl CMCO system.

3.5.3. Proposed mechanism of MgAl CMCO system

To demonstrate the catalytic activity enhancement by the nanoconfined MgAl CMCO system, the first-order rate constant (k) of both 15-MgAl CMCO and non-confined heterogeneous catalytic ozonation under the same experiment condition ($C_{Ibuprofen}$= 5 mg/L; ozone dosage= 2 mg/L) was evaluated. As shown in Fig. S19, the k value of MgAl CMCO (0.449 min^{-1}) is 1.89 times of the k value for non-confined heterogeneous catalytic ozonation (0.238 min^{-1}). These results implied that the

nanoconfined MgAl CMCO system could increase the efficiency of catalytic ozonation. The pore size of 15-MgAl membrane was around 152 nm (Fig. S20), which was near the critical effective diffusion length of short-lived HO· radicals [38]. The catalysts embedded in membrane pores provided active sites for the generation of HO· by decomposing ozone molecules and the confined space facilitated the high availability of HO· for non-selective destruction of organic pollutants. The nanoconfinement within 15-MgAl membrane pores could also enhance the concentration of reactants, promote mass diffusion and enhance the interaction between ozone molecules and catalyst, thus facilitating the reaction kinetics.

The degradation mechanism of organic pollutants by MgAl CMCO was proposed in Fig. 7 based on the experiments and characterizations above. First, the $MgAl_2O_4$ catalyst surface was covered by hydroxyl groups (Me-OH) by interacting with water molecules. According to pH_{pzc} test, $MgAl_2O_4$ exhibited strong basicity with pH_{pzc} of 9.0. As a consequence, the positively charged $Me-OH_2^+$ on the surface of $MgAl_2O_4$ became predominant and acted as Lewis acid sites. Second, due to the resonance structure of ozone molecule, the terminal oxygen atoms in ozone were electron-rich [39], which indicated that the positively charged $Me-OH_2^+$ could function as active sites to attract ozone molecules. Initially, the ozone molecules were bonded with $Me-OH_2^+$ by hydrogen bond or electrostatic force to form $Me-OH_2^+(O_3)$ (Eqs. (3 and 4)). Further, $Me-OH_2^+(O_3)$ would go through surface $Me-·OH^+$ by electron transfer while releasing $HO_3·$ into bulk solution (Eq. (5)). The $Me-·OH^+$ could interact with H_2O molecules to regenerate the surface $Me-OH_2^+$ (Eq. (6)). The released $HO_3·$ would initiate chain reactions to generate HO· by reacting with ozone and its intermediates (Eqs. (7–13)).
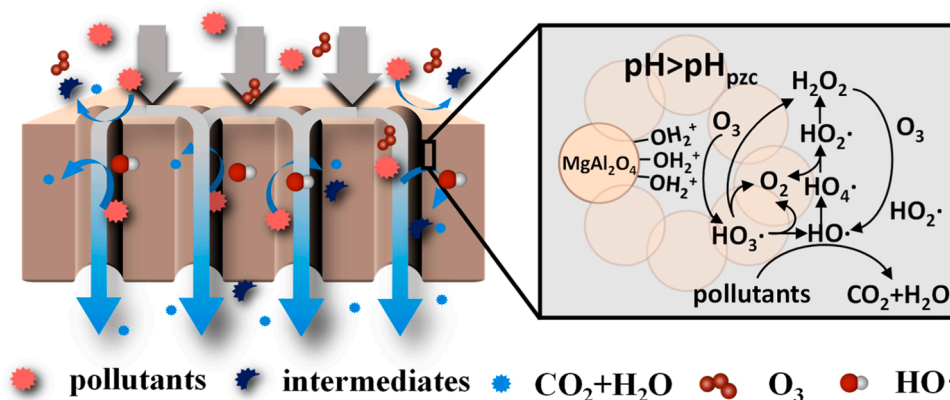
$$Me - OH_2^+ + O_3 \underset{\text{Hydrogen bond}}{\rightarrow} Me - OH_2^+ (O_3) \tag{3}$$

$$Me - OH_2^+ + O_3 \underset{\text{Electrostatic force}}{\rightarrow} Me - OH_2^+ (O_3) \tag{4}$$

$$Me - OH_2^+ (O_3) \rightarrow Me - ·OH^+ + HO_3· \tag{5}$$

$$Me - O·H^+ + H_2O \rightarrow Me - OH_2^+ + HO· \tag{6}$$

$$HO_3· \rightarrow HO· + O_2 \tag{7}$$

$$HO· + O_3 \rightarrow HO_4· \tag{8}$$

$$HO_4· \rightarrow HO_2· + O_2 \tag{9}$$

$$2HO_2· \rightarrow H_2O_2 + O_2 \tag{10}$$

$$HO_3· + HO_3· \rightarrow H_2O_2 + 2O_2 \tag{11}$$

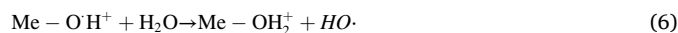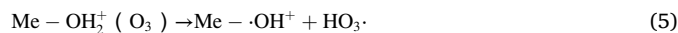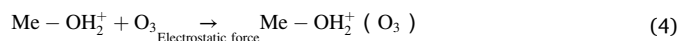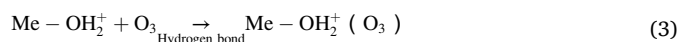$$H_2O_2 + O_3 \rightarrow HO· + HO_2· + O_2 \tag{12}$$

Fig. 7. Schematic illustration and proposed mechanism of catalytic ozonation of organic pollutants in MgAl membrane coupled with ozonation.

$$H_2O_2 + HO_2 \cdot \rightarrow HO\cdot + H_2O + O_2 \qquad (13)$$

4. Conclusion

In this study, a nanoconfined catalytic ceramic membrane was successfully fabricated by incorporating $MgAl_2O_4$ catalyst into the nanopores of membrane. The MgAl membrane exhibited effective catalytic ozonation of refractory organic pollutants and stable degradation efficiency in 25 h. EPR and experiment results revealed that HO· was the dominant ROS species in MgAl CMCO system. The surface hydroxyl groups (Me-OH) was identified as the active sites for the decomposition of ozone to HO· generation. This work provides a new insight for efficient pollutant degradation in wastewater treatment under spatial confinement by a membrane-based strategy.

CRediT authorship contribution statement

Haokun Bai: Investigation, Methodology, Data curation, Formal analysis, Writing – original draft. **Lanlan Liang:** Supervision, Resources & Methodology. **Peike Cao:** Investigation, Writing – review & editing. **Haiguang Zhang:** Investigation, Writing – review & editing. **Shuo Chen:** Investigation & Supervision. **Hongtao Yu:** Resources & Methodology. **Xie Quan:** Project administration, Supervision, Writing – review & editing, Funding acquisition.

Declaration of Competing Interest

The authors declare that they have no known competing financial interests or personal relationships that could have appeared to influence the work reported in this paper.

Acknowledgements

Appendix A. Supporting information

Supplementary data associated with this article can be found in the online version at doi:10.1016/j.apcatb.2023.123527.

References

[1] Q. Guo, C. Zhou, Z. Ma, X. Yang, Fundamentals of TiO_2 photocatalysis: concepts, mechanisms, and challenges, Adv. Mater. 31 (2019), 1901997.

[2] Y. Liu, Y. Zhao, J. Wang, Fenton/Fenton-like processes with in-situ production of hydrogen peroxide/hydroxyl radical for degradation of emerging contaminants: advances and prospects, J. Hazard. Mater. 404 (2021), 124191.

[3] Y. Gao, Y. Zhu, T. Li, Z. Chen, Q. Jiang, Z. Zhao, X. Liang, C. Hu, Unraveling the high-activity origin of single-atom iron catalysts for organic pollutant oxidation via peroxymonosulfate activation, Environ. Sci. Technol. 55 (2021) 8318–8328.

[4] S. Wang, Y. Tian, Z. Wang, Q. Wang, J. Jia, X. Hao, S. Gao, F. Cui, Integrated process for membrane fouling mitigation and organic pollutants removal using copper oxide modified ceramic hollow fiber membrane with in-situ peroxymonosulfate activation, Chem. Eng. J. 396 (2020), 125289.

[5] G. Yu, Y. Wang, H. Cao, H. Zhao, Y. Xie, Reactive oxygen species and catalytic active sites in heterogeneous catalytic ozonation for water purification, Environ. Sci. Technol. 54 (2020) 5931–5946.

[6] S. Afzal, X. Quan, J. Zhang, High surface area mesoporous nanocast $LaMO_3$ (M=Mn, Fe) perovskites for efficient catalytic ozonation and an insight into probable catalytic mechanism, Appl. Catal. B Environ. 206 (2017) 692–703.

[7] D. Liu, C. Wang, Z. Wang, Y. Sun, X. Liu, S. Xiao, L. Li, J. Zhou, Magnetically separable $NiFe_2O_4$/sepiolite catalyst for enhanced ozonation treatment of quinoline and bio-treated coking wastewater in a catalytic ozonation system, Process Saf. Environ. Prot. 159 (2022) 422–432.

[8] Y. Bai, Y.-H. Wu, Y.-H. Wang, X. Tong, X.-H. Zhao, N. Ikuno, H.-Y. Hu, Membrane fouling potential of the denitrification filter effluent and the control mechanism by ozonation in the process of wastewater reclamation, Water Res. 173 (2020), 115591.

[9] J. Wang, X. Quan, S. Chen, H.T. Yu, G.B. Liu, Enhanced catalytic ozonation by highly dispersed CeO_2 on carbon nanotubes for mineralization of organic pollutants, J. Hazard. Mater. 368 (2019) 621–629.

[10] Z. Zhang, H. Ai, M.-L. Fu, Y.-b Hu, J. Liu, Y. Ji, V. Vasanthakumar, B. Yuan, Oxygen vacancies enhancing performance of Mg-Co-Ce oxide composite for the selective catalytic ozonation of ammonia in water, J. Hazard. Mater. (2022), 129000.

[11] S. Zhang, X. Quan, D. Wang, Catalytic ozonation in arrayed zinc oxide nanotubes as highly efficient mini-column catalyst reactors (MCRs): augmentation of hydroxyl radical exposure, Environ. Sci. Technol. 52 (2018) 8701–8711.

[12] L. Chen, Z. Yang, J. Qian, B. Pan, Interaction between organic compounds and catalyst steers the oxidation pathway and mechanism in the iron oxide-based heterogeneous Fenton system, Environ. Sci. Technol. 56 (2022) 14059–14068.

[13] Z. Wang, Z. Si, D. Cai, G.L. Shufeng Li, P. Qin, Synthesis of stable COF-300 nanofiltration membrane via in-situ growth with ultrahigh flux for selective dye separation, J. Membr. Sci. 615 (2020), 118466.

[14] P. Árki, C. Hecker, G. Tomandl, Y. Joseph, Streaming potential properties of ceramic nanofiltration membranes – Importance of surface charge on the ion rejection, Sep. Purif. Technol. 212 (2019) 660–669.

[15] Y. Yang, H. Wang, J. Li, B. He, T. Wang, S. Liao, Novel functionalized nano-TiO_2 loading electrocatalytic membrane for oily wastewater treatment, Environ. Sci. Technol. 46 (2012) 6815–6821.

[16] Y. Yang, W. Fu, X. Chen, L. Chen, C. Hou, T. Tang, X. Zhang, Ceramic nanofiber membrane anchoring nanosized Mn_2O_3 catalytic ozonation of sulfamethoxazole in water, J. Hazard. Mater. 436 (2022), 129168.

[17] Y. He, L. Wang, Z. Chen, X. Huang, X. Wang, X. Zhang, X. Wen, Novel catalytic ceramic membranes anchored with MnMe oxide and their catalytic ozonation performance towards atrazine degradation, J. Membr. Sci. 648 (2022), 120362.

[18] W.J. Lee, Y. Bao, C. Guan, X. Hu, T.-T. Lim, Ce/TiO_x-functionalized catalytic ceramic membrane for hybrid catalytic ozonation-membrane filtration process: fabrication, characterization and performance evaluation, Chem. Eng. J. 410 (2021), 128307.

[19] H. Bader, J. Hoigné, Determination of ozone in water by the indigo method, Water Res. 15 (1981) 449–456.

[20] M. Han, Z. Wang, Y. Xu, R. Wu, S. Jiao, Y. Chen, S. Feng, Physical properties of $MgAl_2O_4$, $CoAl_2O_4$, $NiAl_2O_4$, $CuAl_2O_4$, and $ZnAl_2O_4$ spinels synthesized by a solution combustion method, Mater. Chem. Phys. 215 (2018) 251–258.

[21] F. Bosi, U. Hålenius, V. D'Ippolito, G.B. Andreozzi, Blue spinel crystals in the $MgAl_2O_4$-$CoAl_2O_4$ series: part II. Cation ordering over short-range and long-range scales, Am. Mineral. 97 (2012) 1834–1840.

[22] W. Zha, Z. Zhou, D. Zhao, S. Feng, Positive effects of Al^{3+} partially substituted by Co^{2+} cations on the catalytic performance of $Co_{1+x}Al_{2-x}O_4$ (x = 0–0.2) for methane combustion, J. Sol. Gel Sci. Technol. 78 (2016) 144–150.

[23] H. Song, J. Shao, Y. He, B. Liu, X. Zhong, Natural organic matter removal and flux decline with PEG–TiO_2-doped PVDF membranes by integration of ultrafiltration with photocatalysis, J. Membr. Sci. 405–406 (2012) 48–56.

[24] Y. Guo, B. Xu, F. Qi, A novel ceramic membrane coated with MnO_2-Co_3O_4 nanoparticles catalytic ozonation for benzophenone-3 degradation in aqueous solution: fabrication, characterization and performance, Chem. Eng. J. 287 (2016) 381–389.

[25] Q. Gu, T.C.A. Ng, Y. Bao, H.Y. Ng, S.C. Tan, J. Wang, Developing better ceramic membranes for water and wastewater treatment: where microstructure integrates with chemistry and functionalities, Chem. Eng. J. 428 (2022), 130456.

[26] W.J. Lee, Y.P. Bao, X. Hu, T.T. Lim, Hybrid catalytic ozonation-membrane filtration process with CeO_x and MnO_x impregnated catalytic ceramic membranes for micropollutants degradation, Chem. Eng. J. 378 (2019), 121670.

[27] Z. Wang, Z. Chen, J. Chang, J. Shen, J. Kang, Q. Chen, Fabrication of a low-cost cementitious catalytic membrane for p-chloronitrobenzene degradation using a hybrid ozonation-membrane filtration system, Chem. Eng. J. 262 (2015) 904–912.

[28] X.X. Cheng, H. Liang, F.S. Qu, A. Ding, H.Q. Chang, B. Liu, X.B. Tang, D.J. Wu, G. B. Li, Fabrication of Mn oxide incorporated ceramic membranes for membrane fouling control and enhanced catalytic ozonation of p-chloronitrobenzene, Chem. Eng. J. 308 (2017) 1010–1020.

[29] D. Xu, T. Ding, Y. Sun, S. Li, W. Jing, Interlayer-confined two-dimensional manganese oxide-carbon nanotube catalytic ozonation membrane for efficient water purification, Front. Chem. Sci. Eng. 16 (2022) 731–744.

[30] L. Zhao, Z. Sun, J. Ma, Novel relationship between hydroxyl radical initiation and surface group of ceramic honeycomb supported metals for the catalytic ozonation of nitrobenzene in aqueous solution, Environ. Sci. Technol. 43 (2009) 4157–4163.

[31] L. Zhao, Z. Sun, J. Ma, H. Liu, Enhancement mechanism of heterogeneous catalytic ozonation by cordierite-supported copper for the degradation of nitrobenzene in aqueous solution, Environ. Sci. Technol. 43 (2009) 2047–2053.

[32] Y. Zhao, D. Lu, Y. Cao, S. Luo, Q. Zhao, M. Yang, C. Xu, J. Ma, Interaction analysis between gravity-driven ceramic membrane and smaller organic matter: implications for retention and fouling mechanism in ultralow pressure-driven filtration system, Environ. Sci. Technol. 52 (2018) 13718–13727.

[33] C. Li, W. Sun, Z. Lu, X. Ao, C. Yang, S. Li, Systematic evaluation of TiO_2-GO-modified ceramic membranes for water treatment: retention properties and fouling mechanisms, Chem. Eng. J. 378 (2019), 122138.

[34] K.-i Ishibashi, A. Fujishima, T. Watanabe, K. Hashimoto, Quantum yields of active oxidative species formed on TiO_2 photocatalyst, J. Photochem. Photobiol. Chem. 134 (2000) 139–142.

[35] J. Hoigné, H. Bader, Rate constants of reactions of ozone with organic and inorganic compounds in water—I: non-dissociating organic compounds, Water Res. 17 (1983) 173–183.

[36] M. Sui, L. Sheng, K. Lu, F. Tian, FeOOH catalytic ozonation of oxalic acid and the effect of phosphate binding on its catalytic activity, Appl. Catal. B Environ. 96 (2010) 94–100.

[37] H. Zhao, Y. Dong, P. Jiang, G. Wang, J. Zhang, K. Li, An insight into the kinetics and interface sensitivity for catalytic ozonation: the case of nano-sized NiFe$_2$O$_4$, Catal. Sci. Technol. 4 (2014) 494–501.

[38] S. Zhang, M. Sun, T. Hedtke, A. Deshmukh, X. Zhou, S. Weon, M. Elimelech, J.-H. Kim, Mechanism of heterogeneous fenton reaction kinetics enhancement under nanoscale spatial confinement, Environ. Sci. Technol. 54 (2020) 10868–10875.

[39] T. Ren, M. Yin, S. Chen, C. Ouyang, X. Huang, X. Zhang, Single-atom Fe-N$_4$ sites for catalytic ozonation to selectively induce a nonradical pathway toward wastewater purification, Environ. Sci. Technol. 57 (2023) 3623–3633.